'Inverse Mapping' of Non Thermal Optical Emission from Isolated Neutron Stars

P.O'Connor[1], *A.Shearer*[1], *A.Golden*[1], *S.Eikenberry*[2]

1: Astrophysics & Computing Group, N.U.I. Galway, Ireland
2: Dept. of Astronomy, Cornell University, Ithaca, N.Y.

December 2000

National University of Ireland, Galway
Ollscoil na hÉireann, Gaillimh

CORNELL
UNIVERSITY

Abstract

There are no clear theories of non thermal pulsar emission in the IR $\rightarrow$ UV energy range.The region within the magnetosphere where these emissions arise is essentially unknown. This work is an attempt to place constraints on possible emission regions using a computationally intensive, 'inveres mapping' approach. If this approach is successful then the restriction of physical parameter space within the magnetosphere from which emission arises should make it viable to propose a more detailed physical model of emission. Initial results for the Crab pulsar (PSR 0531+21) are presented and compared with observational data.

1 Introduction

This work is primarily concerned with non thermal (NT) emission from IR $\rightarrow$ UV. NT pulsar emission theories and simulations have been worked on and developed by numerous individuals and groups over the last 30 years (e.g. Ruderman & Sutherland 1975, Cheng, Ho & Ruderman 1986, Daugherty et. al. 1996, Romani 1996 to mention but a select few).

In approaching the problem of optical emission we assume there is a simple, global emission process occurring within the pulsar magnetosphere (synchrotron radiation - see e.g. Sturrock 1971). We simulate emission from each point on a grid which discretises the magnetosphere. From each point a population of particles (number density given by the Goldreich-Julian density (Goldreich & Julian 1969)) is allowed radiate. Output is recorded in the form of arrays containing phase resolved intensity and polarisation data.

Simulated light-curves are compared to observational data with those best matching the data selected. The origin of the phase resolved photons is used to give an inverse mapping onto physical magnetosphere space. It is hoped that this technique may help to constrain an unknown - a hint at the spatial origin of where these emissions arise.

2 Synchrotron Radiation & Polarization

Extremely relativistic particles moving in a spiral motion around magnetic field lines emit synchrotron radiation (e.g. Ginzburg & Syrovatskii 1965, 1969). This radiation has the property that most of the radiated power is confined to a direction along the particle velocity within a narrow solid angle of order $\approx 1/\gamma$ around this direction. The power emitted per unit frequency can be written in the usual notation (see Rybicki & Lightman 1979) as:

$$\frac{dW_{\perp}}{dtd\omega} = P_{\perp}(\omega) = \frac{\sqrt{3}q^3 B sin(\alpha)}{4\pi mc^2}\left[F(x) + G(x)\right] \tag{1}$$

$$\frac{dW_{||}}{dtd\omega} = P_{||}(\omega) = \frac{\sqrt{3}q^3 B sin(\alpha)}{4\pi mc^2}\left[F(x) - G(x)\right] \tag{2}$$

The projection of these two perpendicular emission modes onto the plane of an observer in the sky produce the emission and polarization states for the observer. The polarization seen from synchrotron radiation is in general elliptical and by keeping track of the orthogonal projection of the E field onto an observers plane it is found that:

$$p_{\nu}(1) = \frac{3}{4\pi^2 r^2}\frac{e^2 B}{mc^2\zeta}(\frac{\nu}{\nu_c})\left(1 - \frac{\phi^2}{\zeta^2}\right)^2\left[K_{2/3}(g_{\nu})\right]^2 \tag{3}$$

$$p_{\nu}(2) = \frac{3}{4\pi^2 r^2}\frac{e^2 B}{mc^2\zeta}(\frac{\nu}{\nu_c})\frac{\phi^2}{\zeta^2}\left(1 - \frac{\phi^2}{\zeta^2}\right)^2\left[K_{1/3}(g_{\nu})\right]^2 \tag{4}$$

where $p_\nu(1)$ and $p_\nu(2)$ are the spectral densities of the radiation emitted in the $\hat{x}$ and $\hat{y}$ directions respectively (Bekefi 1966). From equations ?? and ?? above the general case for polarization is elliptical where linear polarization occurs only for $\zeta = 0$ - i.e. when the observers line of sight crosses the emission cone exactly.

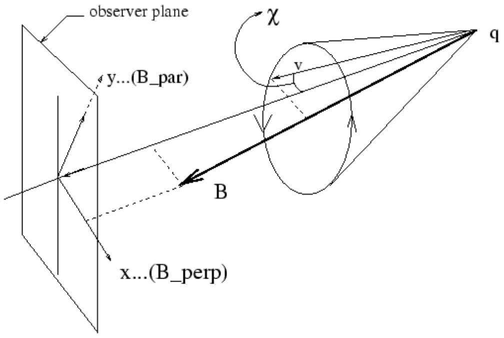

Fig. 1: Polarization projection for synchrotron radiation

3 Model outline

The model used in this work can be divided into essentially two parts:

(a) the modeling of the emission process within the magnetosphere to create observer light-curves and polarisation data which has the following components:

- The magnetic field (B) is given by the Liénard-Wiechert potentials applied to a rotating dipole (the Deutsch field (Deutsch 1955):

$$\vec{B}(\vec{r},t) = \frac{3\hat{r}(\vec{m}.\vec{r}) - \hat{m}}{r^3} + \frac{3\hat{r}(\dot{\vec{m}}.\hat{r}) - \dot{\vec{m}}}{r^2} + \frac{\hat{r} \times (\hat{r} \times \ddot{\vec{m}})}{r} \tag{5}$$

  $\vec{m}$ being the magnetic dipole moment.

- This structure is sampled numerically by imposing a cylindrical mesh (divided radially, azimuthally and in the z-axis direction on a cylindrical co-ordinate system) on the whole magnetosphere and allowing each region to radiate independently.
- The local density of electrons/positrons is taken to be that calculated by Goldreich & Julian (1969 - GJ69): $N_{GJ} = \mathbf{\Omega}.\mathbf{B}/(2\pi ec)$
- At each point this population of particles is assumed to emit synchrotron radiation alone. The emission pattern onto the sky is essentially a cone. Relevant effects in the magnetosphere include relativistic beaming and the relativistic Doppler shift:

$$\omega = \omega'\gamma(\frac{1}{1 - \beta cos\theta})$$

  which has the effect of (amongst other things) selecting a different set of γ factors from the population which may emit in the optical.

- Formulas ?? and ?? are altered for the motion of the source relative to the observer so that the received power relative to the observer is now:

$$\frac{dW}{dtd\omega} = P(\omega) = \frac{\sqrt{3}q^3 B sin(\alpha)}{4\pi mc^2} [F(x)] \frac{(1-\beta\mu)^4}{\gamma^4} \tag{6}$$

- The polarization as seen from synchrotron radiation was given in equations ?? and ??.
- We observe that for the optical pulsars the total emission over the optical wavelength regions obeys a power law (e.g. Golden et. al. 2000). If the power law of the overall spectral emission is η ($P(\omega) \propto \omega^{-\eta}$) then for a synchrotron source the local source particle distribution is also a power law with:

  $$N(\gamma)d\gamma = C\gamma^{-p}d\gamma, \quad \gamma_1 < \gamma < \gamma_2 \tag{7}$$

  where:

  $$\eta = \frac{p-1}{2} \tag{8}$$

  For the simulations carried out we assume the local particle distribution obeys such a power law.

(b) the 'inverse mapping' of this information back within the magnetosphere in order to create a view of regions which are responsible for the observed output.

- The simulated light-curves are compared to observational data and the source regions of the 'best fit' data are recorded.
- Presently the source regions are presented as a plot of the number of emitting points per radial bin as one moves through the magnetosphere to the light cylinder (see figure 5).

In this way we can attempt to constrain (α, χ) parameter space and isolate regions within the magnetosphere likely to be the source of optical emission.

4 Geometry

To produce output to compare to observational data the simulations must be run over the parameter space associated with the geometry of neutron star emission. The neutron star spin ($\mathbf{\Omega}$) and magnetic (μ) axes can in theory be offset at any angle (denoted α) to each other i.e. α is such that $0 < \alpha < \pi$ (see figure 2). Observers geometry has a similar degeneracy as observer angle (χ) relative to the stars spin axis (Ω) can vary from $0 \rightarrow \pi$.

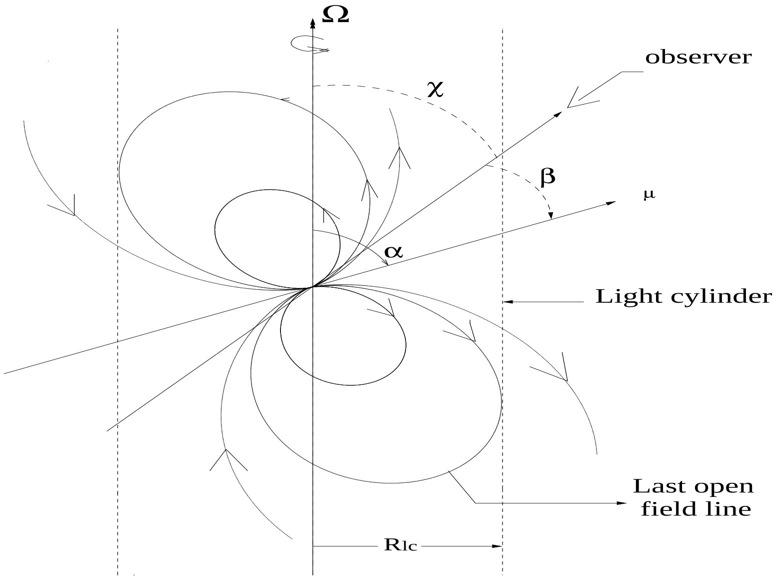

Fig. 2: Generic picture of an inclined dipole

5 Results

There exists some restrictions on individual pulsar χ and α values from radio data and theory (e.g. Lyne & Manchester et. al. 1988 (LM88), Rankin 1990) but these values do not in general agree with each other. In light of this no a priori assumptions are made as regards α or χ and simulations sampled all parameter space in χ for specific inclination values, α. Likewise no assumptions are made as regards a one pole vs two pole emitter, as this should be decided by the model geometry and simulations.

In order to select 'viable' χ values constraints are taken from observational data. The constraints used consist of the phase of the pulsar main peak(s) relative to the radio ($\Delta\phi_R$) and the relative phase separation of the peaks in the energy band of interest ($\Delta\phi_P$). For the Crab pulsar these would be: $\Delta\phi_R \approx 0.12, \Delta\phi_P \approx 0.4$ (Golden 1999) (see figure 3 below - in this figure $\phi = 0$ represents the position of the radio precursor).

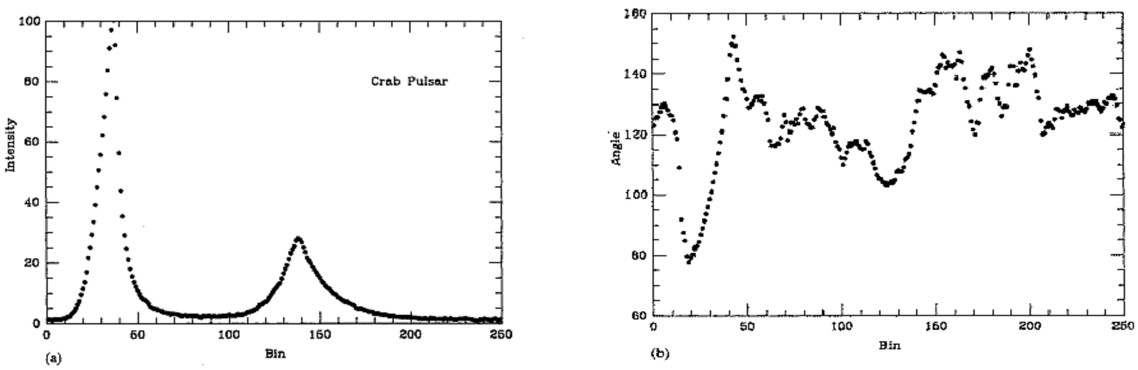

Fig. 3: Observed light-curve and polarization for the Crab (Smith 1988)

'Lightcurves' for different values of χ varied from single to triple-peaked to relatively uniform in profile. This is to be expected as only certain regions of the magnetosphere are visible for different values of χ. Thus far simulation results have not shown an exact phase match with observations. The tolerance of the phase locking algorithm was loosened and some results were then obtained - see figure 4.

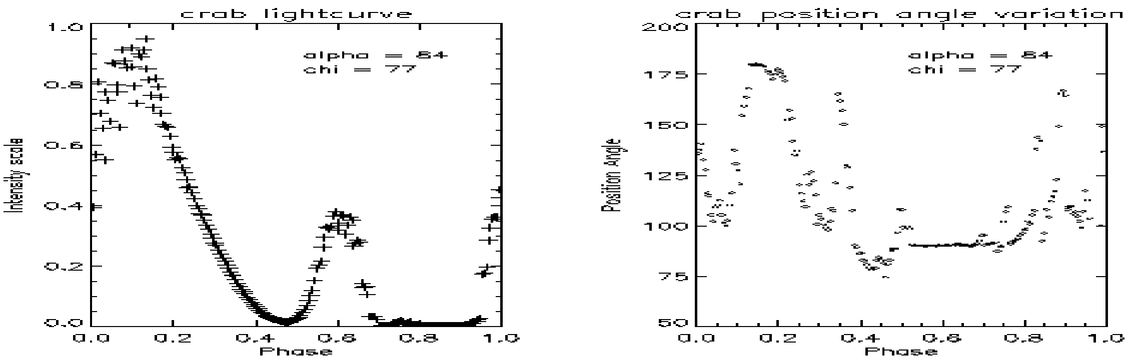

Fig. 4: Simulated light-curve and polarisation position angle swing for Crab like parameters

One can see that the simulation reproduces a double peaked light-curve with peaks of varying intensity, the first in phase of greater intensity than the second. The interpeak phase separation is $\approx 10\%$ more than observed but with $\Delta\phi_{R_{model}} \approx \Delta\phi_{R_{obs.}}$. As can be seen $\Delta\phi_{P_{model}} \approx 0.5$. The rise and fall time of the modeled peaks and the integrated area under the peaks is much different for the model and observations (see Eikenberry 1997b). The polarization angle variation is reproduced to first order across the main peak with a similar range in angle variation but is not similar for the second half of phase.

The inverse mapping of emission regions is shown in figure 5. It represents in one dimension the scaled relative number of points emitting as a function of radial distance from the rotation axis - this number is a summation of points azimuthally and in the $\pm\Omega$ direction. As can be seen, for this particular orientation ($\alpha = 84^o, \chi = 77^o$) emission is confined mainly outside ≈ 0.4 - 0.5 distance to the lightcylinder. Within the context of this model this represents a probability distribution to be further refined by more detailed simulations so in effect one could interpret this result also as there being a very high probability that the emission arises beyond a weighted-average point at ≈ 0.8 x lightcylinder radius - at present this correlates with the Pacini et. al. (1971, 1987) model for optical pulsar emission.

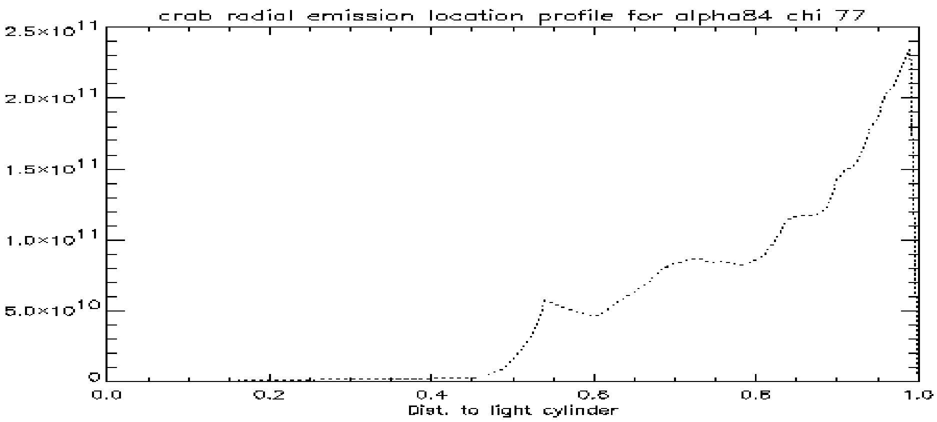

Above: Radial plot of emission points for $\alpha = 84^o \quad \chi = 77^o$

6 Discussion / Conclusions

At present this inverse mapping approach is in it's infancy. Although it reproduces only to first order the observational features mentioned above we interpret the morphological correlations of the simulations as indicative that this approach has potential (it is also promising that LM estimate an α of $\approx 85^o$ for the Crab). Initial results seem to indicate a propensity for emission preferentially at large radial distances from the stellar rotation axis for high α values. This would seem to be in agreement with a recent phenomenological paper (Shearer et. al. 2000) indicating that peak optical emission scales in relation to the B field strength at the light cylinder.

Acknowledgments

P. O' Connor, A. Golden and A. Shearer are grateful for grants received from the National University of Ireland and also Enterprise Ireland.

Bibliography

Bekefi, G., Radiation processes in Plasmas, J. Wiley & sons, Inc., 1966
Chen, K., Chang, H-K, Ho. C., 1996, 471, 967
Cheng,K. S., Ho, C., & Ruderman, M. 1986, Ap. J. 300, 500
Daugherty, J. K., and Harding, A. K. 1996, Ap.J. 458, 270
Deutsch, A. J., 1955, Ann., d'Ap., 18, 1
Eikenberry, S. S., Fazio, G. G., Ransom, S. M., Middleditch, J., Kristian, J., Pennypacker, C.R., 1997b, Ap. J., 447, 465
Ginzburg, V. L., Syrovatskii, S. I., 1965, ARA&A, 3, 297G
Ginzburg, V. L., Syrovatskii, S. I.,1969, ARA&A, 7, 375G
Golden, A., Shearer, A., Beskin, G. M., 2000ApJ, 535, 373G
Golden, 1999, Ph.D. Thesis, NUIGalway, Ireland
Goldreich, P. & Julian, H. 1969, Ap.J., 157, 869
Lyne, A. G., Manchester, R. N. 1988, MNRAS 234, 477L (LM88)
Pacini, F. 1971, ApJ 163L, 17P
Pacini, F., Salvati, M. 1987, ApJ, 321, 447P
Radhakrishnan, V., Cooke, D. J., 1969, ApL, 3, 225R
Rankin, J. M. 1990, 1990ApJ, 352, 247R
Romani, R. W., Yadigaroglu, I. A., 1995, Ap.J. 438, 314
Romani, R. W., 1996, Ap.J. 470, 469
Romani, R. W., 1998, AAS...192.5003R,
Ruderman, M. A., Sutherland, P. G. 1975, ApJ. 196, 51R
Rybiki, G. B., & Lightman, A. P., Radiative Processes in Astrophysics, 1979
Shearer, A. & Golden, A., Accepted for publication by Ap. J. 2000
Smith, F. G., Jones, D. H. P., Dick, J. S. B., Pike, C. D. 1988, MNRAS, 233, 305S
Sturrock, P. A., 1971, ApJ, 164, 529S

1 Astrophysics & Computing Group, National University of Ireland, Galway

2 Department of Astronomy, Cornell University, Ithaca, N.Y.